A&A 526, A122 (2011)
DOI: 10.1051/0004-6361/201015561

Astronomy & Astrophysics

AX J1910.7+0917 and three newly discovered *INTEGRAL* sources

L. Pavan[1,2], E. Bozzo[1,2], C. Ferrigno[1,2], C. Ricci[1,2], A. Manousakis[1,2], R. Walter[1,2], and L. Stella[3]

[1] ISDC, INTEGRAL Science Data Centre, Université de Genève, Chemin d'Ecogia 16, 1290 Versoix, Switzerland
e-mail: lucia.pavan@unige.ch
[2] Observatoire de Genève, Université de Genève, Chemin des Maillettes 51, 1290 Sauverny, Switzerland
[3] INAF – Osservatorio Astronomico di Roma, via Frascati 33, 00044 Rome, Italy

Received 10 August 2010 / Accepted 27 November 2010

ABSTRACT

Aims. We take advantage of the high sensitivity of the IBIS/ISGRI telescope and the improvements in the data analysis software to investigate the nature of the still poorly known X-ray source AX J1910.7+0917, and search for closeby previously undetected objects.
Methods. We analyze all publicly available *INTEGRAL* data of AX J1910.7+0917, together with a number of archival observations that were carried out in the direction of the source with *Chandra*, *XMM-Newton*, and *ASCA*. In the IBIS/ISGRI field-of-view around AX J1910.7+0917, we discovered three new sources: IGR J19173+0747, IGR J19294+1327 and IGR J19149+1036; the latter is positionally coincident with the *Einstein* source 2E 1912.5+1031. For the first two sources, we also report the results of follow-up observations carried out with *Swift*/XRT.
Results. AX J1910.7+0917 features a clear variability in the X-rays. Its spectrum can be well described with an absorbed ($N_{\rm H} \sim 6 \times 10^{22}$ cm^{-2}) power-law ($\Gamma \simeq 1.5$) model plus an iron line at 6.4 keV. We also obtained a refined position and report on possible infrared counterparts.
Conclusions. The present data do not allow for a unique classification of the sources. Based on the property of its X-ray emission and the analysis of a likely infrared counterpart, we investigate different possibilities for the nature of AX J1910.7+0917.

Key words. X-rays: individuals: AX J1910.7+0917 – X-rays: individuals: IGR J19173+0747 – X-rays: individuals: IGR J19294+1327 – X-rays: individuals: IGR J19149+1036 – X-rays: individuals: 2E 1912.5+1031

1. Introduction

The wide field-of-view of the IBIS/ISGRI telescope (FOV, 19°×19°; Ubertini et al. 2003) onboard *INTEGRAL* (Winkler et al. 2003) and its unprecedented sensitivity in the hard X-ray domain (17−100 keV) have made this instrument particularly successful in the past few years in revealing new high-energy sources. The latest available IBIS/ISGRI catalog contains more than 700 objects (Bird et al. 2010) and an increasing number of sources are being discovered thanks to ongoing *INTEGRAL* surveys of the high-energy sky. Since 2003, the relatively large exposure time available (∼1−6 Ms) permitted to achieve in the galactic plane a limiting sensitivity of ≲1 mCrab in the 17−100 keV energy range and a point-source location accuracy of ≃2−3 arcmin. Besides the increasing amount of observing time, the identification of a number of new hard X-ray sources has benefited from improvements in the data analysis software.

In this paper, we take advantage of the new version of the *INTEGRAL* OSA software released by the ISDC (Courvoisier et al. 2003) to investigate the nature of the still poorly known source AX J1910.7+0917, and search for nearby previously undetected faint X-ray sources in the field-of-view (FOV) around this source. In Sect. 2 we summarize all previous observations of AX J1910.7+0917 and the analysis of all the publicly available *INTEGRAL* data. We also carried out an analysis of all archival *Chandra*, *XMM-Newton*, and *ASCA*, observations that included AX J1910.7+0917 in the instruments' FOVs. The analysis of the *INTEGRAL* data also led to the discovery of three new hard X-ray sources in the IBIS/ISGRI FOV around AX J1910.7+0917, independently detected through data analysis also with the BAT_IMAGER software (A. Segreto, priv. comm.). For two of these sources, we obtained follow-up observations with *Swift*/XRT and present these results in Sect. 3. Our discussion and conclusion are summarized in Sect. 4.

2. AX J1910.7+0917

AX J1910.7+0917 is a relatively faint and poorly known X-ray source discovered with *ASCA* during the survey of the Galactic plane. The best-determined position so far is $\alpha_{\rm J2000} = 19^{\rm h}10^{\rm m}47\overset{\rm s}{.}00$ and $\delta_{\rm J2000} = 09°17'06\overset{''}{.}0$, with an associated error of $57\overset{''}{.}6$ (90% c.l., Sugizaki et al. 2001). The *ASCA* spectrum could be fitted with an absorbed power-law model ($\chi^2_{\rm red}$/d.o.f. = 0.72/10). The measured photon index was $\Gamma = 1.1^{+0.5}_{-0.4}$, for an absorption column density of $N_{\rm H} = (2.6^{+1.4}_{-1.0}) \times 10^{22}$ cm^{-2}. The estimated 0.7−10 keV X-ray flux was 2.4×10^{-12} erg/cm^{-2}/s. Sugizaki et al. (2001) associated AX J1910.7+0917 to the *Einstein* source 2E 1908.3+0911, which is characterized by an averaged X-ray flux of $(6.9 \pm 1.4) \times 10^{-13}$ erg/cm^2/s (0.2−3.5 keV, Hertz & Grindlay 1988). The source was also detected with *INTEGRAL*, and classified by Bird et al. (2010) as a likely variable source. The source maximum detection significance in the IBIS/ISGRI data is 8.3σ (18−60 keV), and the corresponding time-average flux is 0.4 ± 0.1 mCrab (0.6 ± 0.1 mCrab) in the 20−40 keV (40−100 keV) energy band (corresponding to 3.0×10^{-12} erg/cm^2/s and 5.7×10^{-12} erg/cm^2/s, respectively). No other detections and counterparts in different energy band have been reported so far.

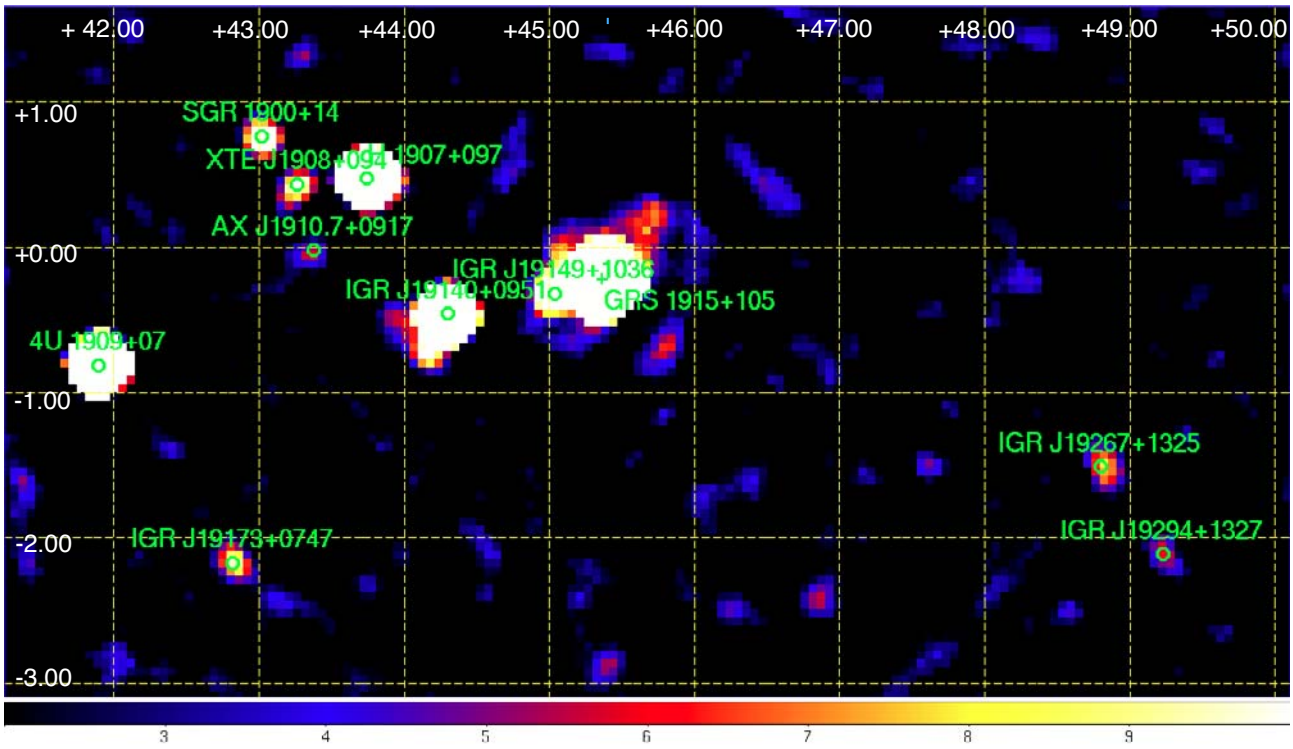

Fig. 1. IBIS/ISGRI mosaic around AX J1910.7+0917 (17–80 keV, significance map). We also show the newly discovered nearby sources (see Sect. 3 and the electronic version of the paper for the colored picture). The dashed grids denote galactic coordinates.

2.1. Data analysis and results

We analyzed all archival *INTEGRAL*, *ASCA*, *XMM-Newton*, and *Chandra* observations that included the position of AX J1910.7+0917 in their FOV. This is the first in-depth study of the emission from this source up to hard X-ray energies. In Sect. 2.1.1 we report the details of the *INTEGRAL* observations. A log of all other observations is given in Table 1. Throughout the paper, all uncertainties are given at 90% c.l. (unless otherwise stated).

2.1.1. *INTEGRAL*

INTEGRAL observations are commonly divided into ∼2–3 ks short pointings called "science windows" (SCWs). We considered all publicly available SCWs for the IBIS/ISGRI (17–80 keV, Lebrun et al. 2003) and for the two JEM-X telescopes (3–23 keV, Lund et al. 2003) that were performed in the direction of AX J1910.7+0917 from 2003 March 6 to 2009 April 15 (see Sect. 2). This permitted us to achieve an effective exposure time on the source of 4.8×10^2 ks and 2.7×10^3 ks for JEM-X and ISGRI respectively. All data, here and below, were analyzed with version 9.0 of the OSA software (Courvoisier et al. 2003).

The source was not detected in the JEM-X1 and JEM-X2 mosaics, and we derived an upper limit on the source X-ray flux by using the tool MOSAIC_SPEC. From the JEM-X1 mosaic we derived a 3σ upper limit of 1.0×10^{-11} erg/cm^2/s, 5.8×10^{-12} erg/cm^2/s, and 9×10^{-12} erg/cm^2/s respectively in the energy bands 3–7 keV, 7–11 keV, and 11–19 keV. The corresponding 3σ upper limits derived from the JEM-X2 mosaic were 1.7×10^{-11} erg/cm^2/s, 1.2×10^{-11} erg/cm^2/s, and 1.8×10^{-11} erg/cm^2/s. These are compatible with the measured averaged *ASCA* flux reported in Sect. 1.

We produced an IBIS/ISGRI mosaic of the region around AX J1910.7+0917, using the energy band 17–80 keV to maximize the S/N. In this energy band AX J1910.7+0917 is detected with a significance of 5.8σ. A close view of the ISGRI mosaic is shown in Fig. 1. We checked that the best-fit position of the source obtained from the mosaic is compatible with both its *ASCA* and *XMM-Newton* refined position (see Sect. 2.1.2).

We derived a count rate of 0.09 ± 0.02 cts/s, corresponding to a flux of 0.31 ± 0.05 mCrab. This flux is higher than any contamination expected in the same energy band from the nearby supernova remnant (SNR, see Miceli et al. 2006, and Sect. 2.1.2).

We also performed a spectral analysis and extracted its lightcurve in the two energy bands 20–40 keV and 40–80 keV. The averaged IBIS/ISGRI spectrum of the source is shown in Fig. 5 and discussed in Sect. 2.1.2. We barycenter-correct the photon arrival times in the source lightcurves with the OSA9 tool BARYCENT. No evidence for a coherent periodicity could be found. This is also confirmed by the analysis of the data from *Swift*/BAT (Cusumano, priv. comm.), which operates in a similar energy band to that of IBIS/ISGRI.

2.1.2. *XMM-Newton*

AX J1910.7+0917 was serendipitously[1] observed in two *XMM-Newton* (Jansen et al. 2001) observations performed in 2004 April in the direction of the nearby SNR W49B (Miceli et al. 2006). We processed *XMM-Newton* observation data files (ODFs) to produce calibrated event lists using the EPPROC and EMPROC tasks (Science Analysis System, SAS, v.10.0) for the Epic-pn and the MOS cameras. The event files of the two observations were filtered to exclude high background time intervals follow-

[1] AX J1910.7+0917 is named as 2XMM J191043.4+091629 in the *XMM-Newton* serendipitous source catalogue (Watson et al. 2009).

Table 1. Observation log of AX J1910.7+0917.

OBS ID	Instr	Date[a]	Exp[b] (ks)	N_H (10^{22} cm^{-2})	Γ	F_{obs}[c] (erg/cm^2/s)	$\chi 2_{red}$/d.o.f. (C-stat/d.o.f.)
ASCA							
50005000	GIS2+GIS3	1993-04-24	95	$4.8^{-1.5}_{+1.9}$	1.4±0.5	$8.2^{+0.7}_{-2.7}$	0.4/53
13000000[d]	GIS2	1993-05-03	2.3	4.8 (fixed)	1.4 (fixed)	<4.2	–
	GIS3	1993-05-03	2.3	4.8 (fixed)	1.4 (fixed)	<4.9	–
13000010[d]	GIS2	1993-05-03	2.3	4.8 (fixed)	1.4 (fixed)	<1.1	–
	GIS3	1993-05-03	2.3	4.8 (fixed)	1.4 (fixed)	<1.6	–
13000030[d]	GIS3	1993-05-03	1.4	4.8 (fixed)	1.4 (fixed)	<2.1	–
	GIS3	1993-05-03	1.4	4.8 (fixed)	1.4 (fixed)	<3.1	–
50005010[d]	GIS2	1993-10-16	12	4.8 (fixed)	1.4 (fixed)	<0.6	–
	GIS3	1993-10-16	12	4.8 (fixed)	1.4 (fixed)	<0.6	–
50005020[d]	GIS2	1993-10-17	20	4.8 (fixed)	1.4 (fixed)	<1.1	–
	GIS3	1993-10-17	20	4.8 (fixed)	1.4 (fixed)	<1.4	–
10020000	GIS2+GIS3	1993-11-03	26	$6.3^{+1.6}_{-1.4}$	2.3±0.5	$4.9^{-4.3}_{+0.4}$	(146.1/157)
10020010[d]	GIS2	1993-11-03	19	4.8 (fixed)	1.4 (fixed)	<2.1	–
	GIS3	1993-11-03	19	4.8 (fixed)	1.4 (fixed)	<2.3	–
57005050	GIS2+GIS3	1999-04-27	23	$5.0^{+3.4}_{-2.4}$	1.6±0.8	$2.5^{+0.2}_{-1.4}$	(70.7/59)
XMM-Newton							
0084100401	Epic-pn	2004-04-03	14.0	$6.3^{+0.5}_{-0.4}$	1.4±0.1	$17.1^{+1.0}_{-2.1}$	1.1/147
0084100501[e]	Epic-pn	2004-04-05	14.7	5.0±0.3	1.28±0.08	$24.3^{+1.2}_{-1.7}$	0.9/168
Chandra							
9615[f]	ACIS-S	2008-05-31	1.7	–	–	<0.4	–

Notes. [a] Format is YYYY-MM-DD; [b] Exp indicates the total exposure time of each observation; [c] observed flux in the 1−10 keV energy band in units of 10^{-12}; [d] 90% c.l. upper limit; [e] this fit includes also a Gaussian line at ∼6.4 keV, see text for details; [f] 68% c.l. upper limit.

ing the reccomandations of the SAS online analysis threads[2]. We excluded from further analysis time intervals in observation 0084100401 (0084100501) during which the count-rate of the entire detector FOV in the 10−12 keV energy band was higher than 0.2 (0.15) cts/s for the Epic-MOS and 0.35 (0.4) for the Epic-pn. We also carefully checked that none of these rises in the total field count-rate was due to a flare from AX J1910.7+0917.

In both observations 0084100401 and 0084100501, the three Epic cameras were operated in full frame and the source AX J1910.7+0917 was located at the rim of their FOV. In the Epic-MOS1 AX J1910.7+0917 lied on the border between two CCDs, and thus we excluded these data from the analysis. The total effective exposure time is of 14.0 ks (18.1 ks) for the Epic-pn (Epic-MOS2) in the observation 0084100401 and 14.7 ks (18.0 ks) in the observation 0084100501. In order to maximize S/N, source lightcurves and spectra were extracted by using an elliptical region (see Fig. 2). As we discuss also below in more detail, the elongated shape of the source is due to the off-axis point spread function of the *XMM-Newton* telescope for sources close to the border of the FOV[3]. Background lightcurves and spectra were extracted in the closest source-free region to AX J1910.7+0917. We checked that none of the results reported in this paper changed significantly by using different (reasonable) source and background extraction regions. We corrected all lightcurves for vignetting, bad pixels, point-spread-function (PSF) losses, and dead time with the SAS EPICLCCORR tool. All EPIC images and spectra were corrected for out of time events,

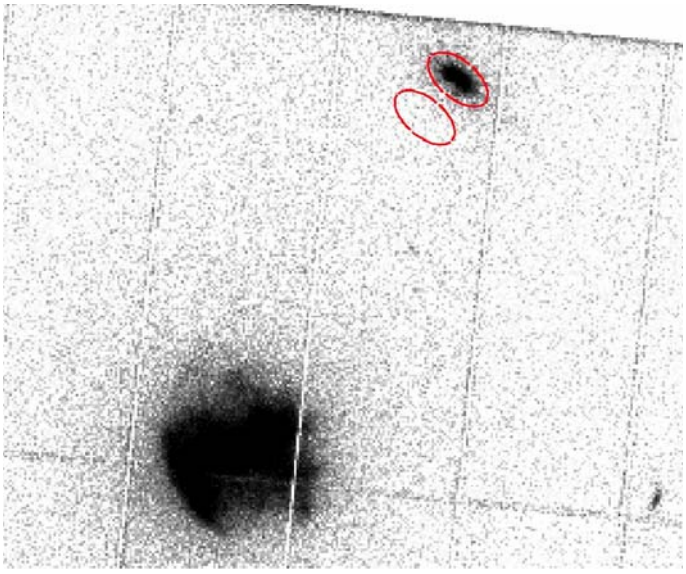

Fig. 2. Image of AX J1910.7+0917 as observed by the Epic-pn detector (0.5−12.0 keV). The extraction region for source and background are also shown. The bright object in the center is the SNR W49B.

according to the instructions provided by the SAS online analysis threads. Epic-pn and Epic-MOS spectra were rebinned before fitting so as to have at least 25 counts per bin and, at the same time, prevent oversampling the energy resolution by more than a factor of three. Given the relatively short exposure time and low X-ray flux of the source, we report below only results from the

[2] http://xmm.esac.esa.int/sas/documentation/threads/.
[3] See also http://xmm.esa.int/external/xmm_user_support/documentation/uhb/node18.html

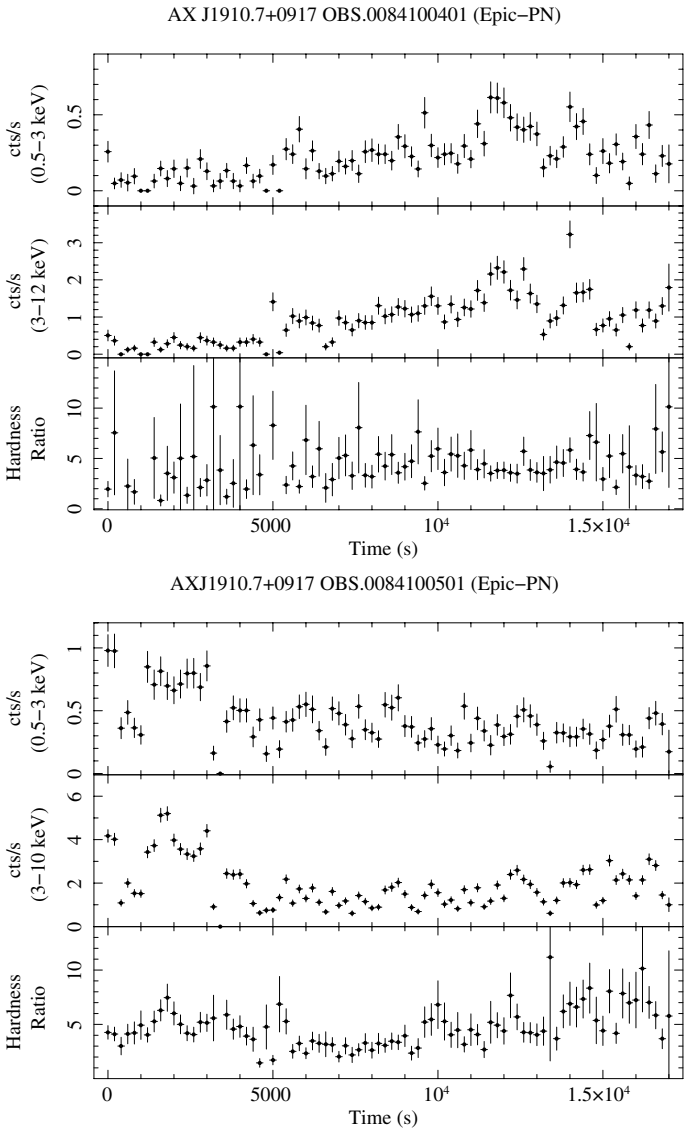

Fig. 3. *XMM-Newton* Epic-pn background-subtracted lightcurves of AX J1910.7+0917 extracted in the two energy bands 0.5−3 keV and 3−12 keV for the two observations 0084100401 (top) and 0084100501 (bottom). The hardness ratio is reported in the bottom panel of each figure. The time bin is 200 s.

Epic-pn analysis and checked that the Epic-MOS2 data would give compatible results in all cases.

In Fig. 3 we report the Epic-pn lightcurves of the source in the 0.5−3 keV and 3−12.0 keV energy bands, extracted from the two *XMM-Newton* observations. The hardness ratio, defined as the ratio of the count rate in the hard (3−12 keV) to soft (0.5−3 keV) energy band versus time, is also shown. A pronounced variability on timescales of hundreds of seconds is clearly visible from these lightcurves, but only marginal variations in the hardness ratio were measured (the most prominent feature is the increase of a factor ∼2 at the beginning of observation 0084100501, see Fig. 3). From the 0.5−12 keV Epic-pn lightcurves in observation 0084100401 (0084100501) we estimated a minimum source count rate of 0.25 ± 0.03 (0.6 ± 0.2) cts/s and a maximum source count rate of 5.6 ± 0.5 (6.2 ± 0.5) cts/s.

In order to search for spectral variations with the source intensity, we extracted from observation 0084100401 two *XMM-Newton* spectra by selecting time intervals in which the source count-rate in the 0.3−12 keV energy band was <2 and >2 cts/s. The first spectrum (effective exposure time 12 ks) could be reasonably well described ($\chi^2_{\rm red}$/d.o.f. = 1.2/125) by using an absorbed power-law (PL) model with $N_{\rm H} = (6.3^{+0.6}_{-0.5}) \times 10^{22}$ cm^{-2} and $\Gamma = 1.4^{+0.2}_{-0.1}$. The estimated 1−10 keV X-ray flux was 1.3×10^{-11} erg/cm^2/s. Alternatively, this spectrum could be well described ($\chi^2_{\rm red}$/d.o.f. = 1.0/125) by using a blackbody (BB) model with a temperature of $kT_{\rm BB} = (1.78 \pm 0.08)$ keV and a radius of $R_{\rm BB} = 0.42 \pm 0.03$ km (for an assumed distance of 10 kpc). The spectrum extracted at higher count-rates (effective exposure time 2 ks) could be reasonably well fitted by using the same models discussed above. This gave $N_{\rm H} = (6.2^{+0.9}_{-0.8}) \times 10^{22}$ cm^{-2}, and $\Gamma = 1.3 \pm 0.2$ for the PL model and $N_{\rm H} = (3.2 \pm 0.5) \times 10^{22}$ cm^{-2}, $kT_{\rm BB} = (2.0 \pm 0.2)$ keV, and $R_{\rm BB} = 0.60 \pm 0.07$ km for the BB model. In this case the estimated flux is 3.8×10^{-11} erg/cm^2/s (1−10 keV). This analysis did not reveal any significant change in the spectral parameters between the higher and lower count-rate spectra. We thus also extracted the average spectrum of this observation (see Fig. 4). This could be well fitted with an absorbed PL model, the parameters of the fit are reported in Table 1. A similar good fit ($\chi^2_{\rm red}$/d.o.f. = 0.9/147) could also be obtained by using a BB model ($kT_{\rm BB} = (1.85 \pm 0.07)$ keV, $R_{\rm BB} = 0.45 \pm 0.03$ km, $N_{\rm H} = (3.3 \pm 0.3) \times 10^{22}$ cm^{-2}).

We carried out a similar analysis for the observation 0084100501. The rate-resolved spectra were extracted during the time intervals in which the source count-rates were >2 and <2 cts/s (0.5−12 keV). We fitted both spectra with an absorbed power-law model and noticed that the residuals from these fits indicated the presence of an iron line at ∼6.4 keV (see Fig. 4). We therefore added a Gaussian line to the spectral model used for the fit. The spectrum extracted at higher count rates (effective exposure time 4.4 ks) gave ($\chi^2_{\rm red}$/d.o.f. = 1.1/134) a power-law photon index of $\Gamma = 1.3 \pm 0.1$, an absorption column density of $N_{\rm H} = (5.3 \pm 0.4) \times 10^{22}$ cm^{-2}, an energy for the iron line centroid of $E_{\rm line} = 6.45 \pm 0.06$ keV and an equivalent width of $EW = 0.06^{+0.04}_{-0.05}$ keV (errors on the EWs are given at 68% c.l. throughout the paper). The normalization of the line was $(3.8 \pm 2.4) \times 10^{-5}$, only yielding an indication of the presence of the line. For this spectrum the estimated 1−10 keV X-ray flux was $(4.3^{+0.1}_{-0.3}) \times 10^{-11}$ erg/cm^2/s. By using a BB model instead of a PL, we obtained $N_{\rm H} = (2.7 \pm 0.3) \times 10^{22}$ cm^{-2}, $kT_{\rm BB} = (1.95 \pm 0.08)$ keV, and $R_{\rm BB} = 0.63 \pm 0.04$ km.

The spectrum extracted at a lower count rate (effective exposure time 10.3 ks) gave $\Gamma = 1.4 \pm 0.1$, $N_{\rm H} = (4.6 \pm 0.4) \times 10^{22}$ cm^{-2}, $E_{\rm line} = 6.42 \pm 0.03$ keV, $EW = 0.14 \pm 0.06$ keV ($\chi^2_{\rm red}$/d.o.f. = 1.0/132), and a flux of $(1.7^{+0.1}_{-0.3}) \times 10^{-11}$ erg/cm^2/s (1−10 keV). The normalization of the line in this case was $(3.3 \pm 1.1) \times 10^{-5}$, thus indicating a detection significance >3σ. By using an absorbed BB instead of the PL component to fit the lower count-rate spectrum in the observation 0084100501 would give $N_{\rm H} = (2.2 \pm 0.2) \times 10^{22}$ cm^{-2}, $kT_{\rm BB} = 1.77 \pm 0.08$ keV, and $R_{\rm BB} = 0.44 \pm 0.03$ km. We also extracted the source spectrum by using the total exposure time of the observation 0084100501. This spectrum is shown in Fig. 4 and the best-fit parameters obtained with an absorbed PL model plus a Gaussian line are reported in Table 1. In this case we found $E_{\rm line} = 6.44 \pm 0.03$ keV and an $EW = 0.09 \pm 0.03$ keV. The normalization of the line was $(3.4 \pm 1.0) \times 10^{-5}$. By using a BB component instead of the PL for this spectrum would give $N_{\rm H} = (2.4 \pm 0.2) \times 10^{22}$ cm^{-2}, $kT_{\rm BB} = 1.85 \pm 0.06$ keV, $R_{\rm BB} = 0.51 \pm 0.03$ km, $\chi^2_{\rm red} = 1.0/168$ and parameters for the iron line fully in agreement (within the errors) with those reported above.

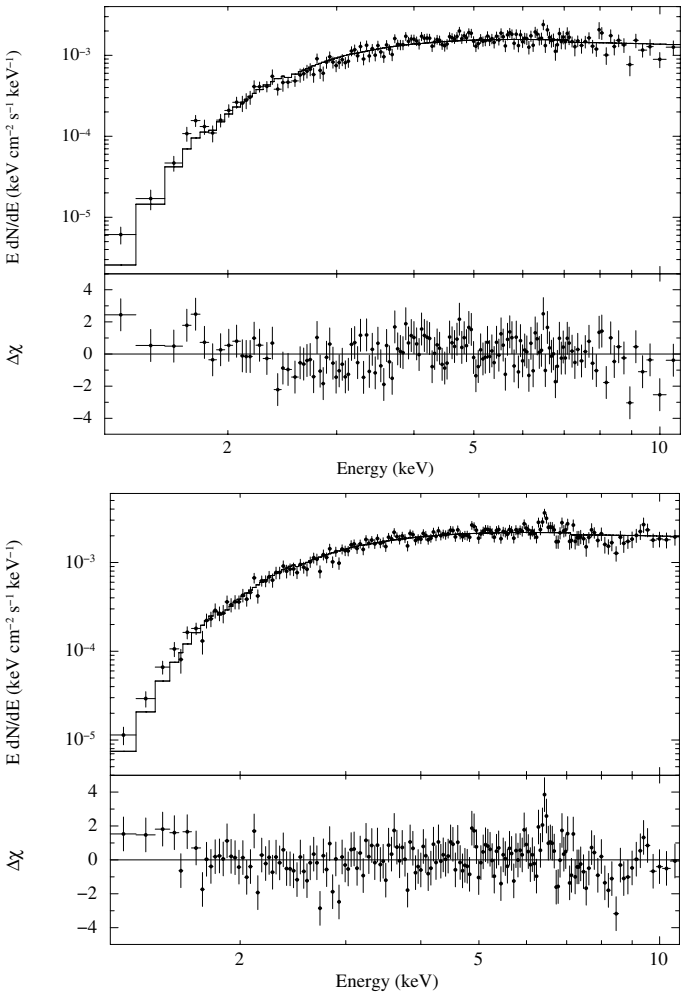

Fig. 4. Averaged *XMM-Newton* Epic-pn spectra of AX J1910.7+0917 extracted from the observations 0084100401 (*top*) and 0084100501 (*bottom*). In both cases we also show the best-fit model (an absorbed power-law) and the residuals from these fits. In the observation 0084100501 the residuals clearly showed an iron line at ~6.4 keV.

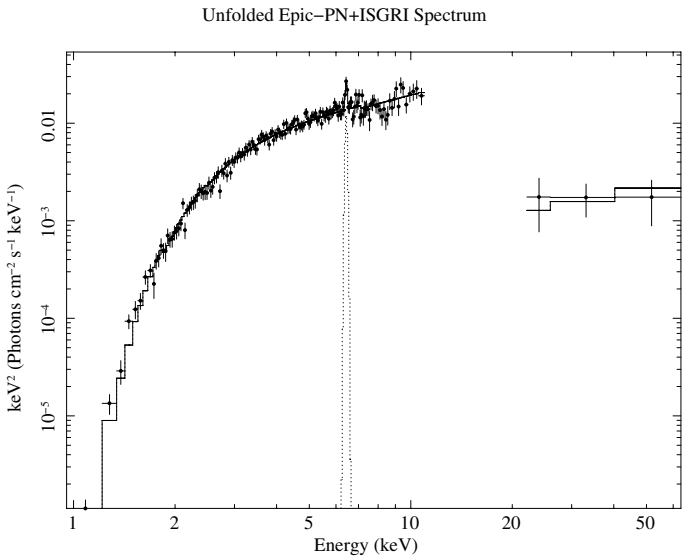

Fig. 5. Unfolded Epic-pn+ISGRI spectrum of AX J1910.7+0917. The best-fit model is obtained with an absorbed power-law model plus a Gaussian line at ~6.4 keV (see text for details).

In order to compare the results found for the two *XMM-Newton* observations of AX J1910.7+0917, we added an iron line with a centroid energy fixed at 6.44 keV to the spectrum extracted by using the total exposure time of observation 0084100401 and determined the 90% c.l. upper limit on its normalization at 1.5×10^{-5}. This value is lower than the one measured in observation 0084100501, but still compatible with that expected due to the lower flux (~40%) of the source in the observation 0084100401. We thus conclude that it is not possible to infer unambiguously from the present data a variation of the iron line parameters between the two observations. Even though no simultaneous *XMM-Newton* and *INTEGRAL* observation were available, we tried a fit to the combined averaged ISGRI spectrum and the Epic-pn averaged spectrum of the observation 0084100501. This spectrum could be well described with an absorbed power law model, and we introduced a normalization constant to take into account both the intercalibration between the Epic-pn and ISGRI instruments and the variability of the source. The values of the absorption column density and power-law photon index were found to be fully consistent with those of the averaged Epic-pn spectrum, but the normalization constant turned out to be 0.04 ± 0.02 (this value would be 0.06 ± 0.03 if the same fit were performed by using the *XMM-Newton* spectrum of the observation 0084100401). The relatively low value of the normalization constant between the two instruments indicates that on average the X-ray flux of the source is much lower than that measured during the *XMM-Newton* observations. This is consistent with the results reported in Table 1. The unfolded Epic-pn+ISGRI spectrum is shown in Fig. 5.

Finally, we also extracted for both *XMM-Newton* observations a spatially resolved X-ray spectrum by selecting different regions centered on the source in order to search for spectral shape variations and investigate a possible extended nature of the source. We did not find any evidence for a significant change in the spectral parameters, and concluded that the elongated shape of the source is most likely caused by distortion of the instrument PSF for sources close to the border of the FOV (see also above). Because of this problem, the determination of an improved source position requires some caution. We used the automatic *XMM-Newton* source-detection task EDETECT-CHAIN (with manually fine-tuned parameters), to have an estimate of the source position and error in the two *XMM-Newton* observations for both the Epic-pn and Epic-MOS2 cameras. In the observation 0084100401, the two best-determined positions are (i) $\alpha_{J2000} = 19^h10^m43\overset{s}{.}42$, $\delta_{J2000} = 09°16'29\overset{''}{.}3$ and (ii) $\alpha_{J2000} = 19^h10^m43\overset{s}{.}37$, $\delta_{J2000} = 09°16'29\overset{''}{.}3$, for the Epic-pn and the Epic-MOS2, respectively. The corresponding positions obtained in the observation 0084100501 were (i) $\alpha_{J2000} = 19^h10^m43\overset{s}{.}44$, $\delta_{J2000} = 09°16'30\overset{''}{.}7$ and (ii) $\alpha_{J2000} = 19^h10^m43\overset{s}{.}39$, $\delta_{J2000} = 09°16'30\overset{''}{.}0$. According to the latest calibration document available, the relative astrometry among all EPIC cameras is estimated to be better than 1.5″, and the absolute astrometric accuracy of any source in the *XMM-Newton* FOV is of ~2″. Only for faint MOS sources near the detection limit this error can be as large as 4″ (90% c.l.). In the present case all results on the positions we obtained are consistent within 1.5″ as expected. Given the position of AX J1910.7+0917 at the very rim of the *XMM-Newton* detector, we assume in the following as the best determined position of the source: $\alpha_{J2000} = 19^h10^m43\overset{s}{.}39$, $\delta_{J2000} = 09°16'30\overset{''}{.}0$ (J2000), with a conservative associated error of 2″ (90% c.l.). In Sect. 2.1.5 we use this result to search for possible counterparts to AX J1910.7+0917.

A Fourier analysis of the *XMM-Newton* data of AX J1910.7+0917 did not reveal any indication for a possible coherent periodicity.

2.1.3. *ASCA*

AX J1910.7+0917 was serendipitously observed in several *ASCA* (Tanaka et al. 1994) observations performed in 1993 and 1999. A log of these observations is provided in Table 1. We used data from the two gas-imaging spectrometers (GIS2 and GIS3, Ohashi et al. 1996; Makishima et al. 1996) and applied standard screening criteria[4]. We extracted the source light curves and spectra from a circular region of 2′ radius. A larger extraction region could not be used because of the emission from the nearby SNR (see also Sect. 2.1.2). For the background, we used a similar extraction region, located in the same part of the FOV as the source events, as described in the *ASCA* ABC guide. Note that AX J1910.7+0917 is located well within the Galactic disk and thus we could not use the *ASCA* blank-sky observations (see p. 80 of the *ASCA* ABC guide). We used the latest available GIS2 and GIS3 instrument response files (gis2v4_0.rmf and gis3v4_0.rmf) and generated for each observation the corresponding ancillary file with the tool ASCAARF.

Only in observation 50 005 000 was the statistics sufficiently high to rebin the spectrum to have at least 20 photons per bin and perform a minimum χ^2 fitting. In all observations where the source was detected but the statistics was relatively poor, the C-statistics was used for the fits. We also determined a 90% c.l. upper limit on the source X-ray flux in all the observations in which AX J1910.7+0917 was not detected. In these cases, we obtained a source and background spectrum by using the same extraction regions adopted in the other observations, and fitted them with an absorbed PL model. The absorption column density and PL photon index were fixed to those of observation 50 005 000, and the 90% c.l. error on the model normalization was used to obtain an upper limit on the flux (1−10 keV energy band). All these results are reported in Table 1. Given the low S/N of the *ASCA* observations of AX J1910.7+0917, we did not investigate possible timing features in these data.

2.1.4. *Chandra*

A research in the HEASARC data archive[5] revealed that AX J1910.7+0917 was also twice observed by the ACIS telescope on-board *Chandra* (Garmire et al. 2003). The first of these observations (ID. 117) was performed on 2001 July 8 and lasted for 54 ks. AX J1910.7+0917 was serendipitously observed in the ACIS-I2 chip, but not detected. Unfortunately, the analysis of this observation revealed the presence of a large number of poorly illuminated columns on the ACIS-I2 chip (most likely a read-out problem), and therefore we did not consider this observation in our subsequent analysis. In the second observation (ID. 9615), performed on 2008 May 31 and lasting 1.65 ks, AX J1910.7+0917 was observed in the FOV of the ACIS-S3 chip, but not detected.

We derived from these data an upper limit on the source X-ray flux by using both the APRATES task[6] available within the CIAO package (v.4.2) and by building a fluxed image of the ACIS-S3 chip[7]. The first method allowed us to derive a 68% c.l. upper limit on the source count rate of 0.012 cts/s (0.5−7 keV), which corresponds to a 1−10 keV X-ray flux of 4.0×10^{-13} erg/cm^2/s (we used the online tool WEBPIMMS[8] and assumed a PL model with $\Gamma = 1.4$ and $N_{\rm H} = 4.8 \times 10^{22}$ cm^{-2} to be consistent with the other upper limits derived, see Sect. 2.1.3). The second method permits us to directly calculate the energy flux in units of erg/cm^2/s for each event in the selected *Chandra* chip, taking into account the quantum efficiency and effective area as well. With this method we estimated a 3σ upper limit on the source X-ray flux of 5.4×10^{-13} erg/cm^2/s (0.5−7 keV) energy band, compatible with the limit derived with the first method.

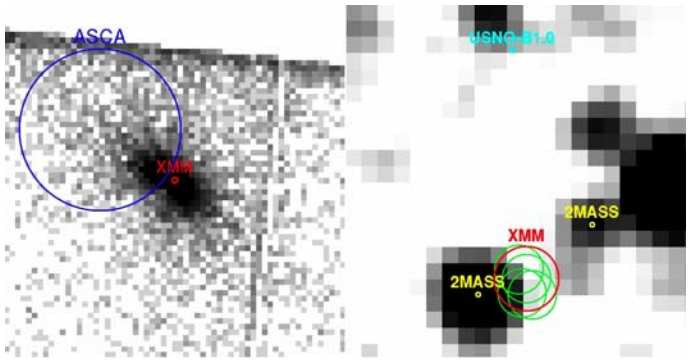

Fig. 6. *XMM-Newton* (*left*) and infrared (2MASS, *J* band, *right*) image of the region around AX J1910.7+0917. We show the error circles (green) associated with the determined positions in the 2 *XMM-Newton* observations for the Epic-pn and Epic-MOS2 cameras, and the best adopted source position (red circle, error 2″ at 90% c.l.). We also show in blue the previously determined *ASCA* position (only slightly outside the *XMM-Newton* error circle) and the closest 2MASS and USNO-B1.0 counterparts discussed in Sect. 2.1.5 (see the electronic version of the paper for the colored picture).

2.1.5. Counterparts of AX J1910.7+0917

We used the improved source position found from the *XMM-Newton* data to search for an infrared and/or optical counterpart to AX J1910.7+0917. In Fig. 6 we show the *XMM-Newton* FOV around AX J1910.7+0917, and the corresponding 2MASS image (Skrutskie et al. 2006). The four determined positions in the *XMM-Newton* observations (green circles) and the best adopted source position (red circle, error 2″ at 90% c.l.) are also shown. We found only one likely counterpart, 2MASS J19104360+0916291, which partly lies within the *XMM-Newton* error circle and has $J = 15.044 \pm 0.030$, $H = 13.000 \pm 0.022$, and $K = 11.808 \pm 0.023$. No cataloged optical counterparts were found within the *XMM-Newton* error circle. The closest object in the USNO-B1.0 catalog is shown in the figure but because of the relatively large separation from AX J1910.7+0917, it is very unlikely that it is associated with AX J1910.7+0917. We note that the lack of a clear optical counterpart is compatible with the high absorption in the direction of the source measured from the *XMM-Newton* observations (see Sect. 2.1.2). We also queried the FIRST Survey and the NVSS catalogs in search for a radio counterpart, but did not find any obvious candidate.

[4] See the ASCA ABC guide at http://heasarc.gsfc.nasa.gov/docs/asca/abc/abc.html.

[5] http://heasarc.gsfc.nasa.gov/.

[6] See the on-line thread: http://cxc.harvard.edu/ciao/threads/aprates/$\protect\kern-.1667em\relax$index.html#netcts.

[7] See the on-line thread: http://cxc.harvard.edu/ciao/threads/eff2evt.

[8] http://heasarc.nasa.gov/Tools/w3pimms.html

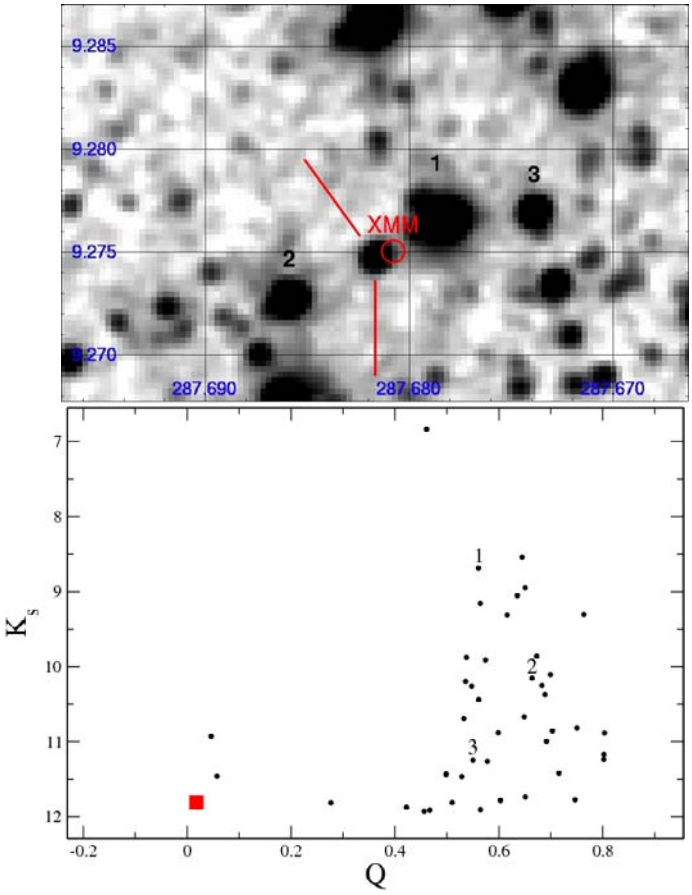

Fig. 7. *Top*: 2MASS image (K band, coordinates in Right Ascension and Declination) of the FOV around AX J1910.7+0917. The best-determined *XMM-Newton* position is marked in red, and a few nearby potential IR candidates are also displayed. *Bottom*: Plot of Q vs. K_s magnitudes for the 2MASS stars around the XMM position (see text for details). The square represents the likely IR counterpart to AX J1910.7+0917. Some of the nearby potential candidates are also shown.

To investigate the nature of the possible IR counterpart found above for AX J1910.7+0917 in more detail, we applied the analysis described in Negueruela & Schurch (2007) to the objects in the FOV of 2MASS J19104360+0916291. For each star represented in Fig. 7 we used 2MASS photometric data to obtain the values of their J, H, and K. Then, we calculated the quantity $Q = (J - H) - 1.70(H - K_s)$ for each object (here $K_s = K$) and plotted these values as a function of K_s in the bottom panel of Fig. 7. According to Negueruela & Schurch (2007), the objects characterized by $K_s \lesssim 11$ and $Q \lesssim 0.2$ are promising supergiant candidates. Even though this method does not provide a secure classification, it suggests that the nature of the source 2MASS J19104360+0916291 (red square in Fig. 7) would be compatible with being a supergiant star. We discuss this aspect further in Sect. 4.

3. New *INTEGRAL* sources

In the IBIS/ISGRI FOV around AX J1910.7+0917, we found three new sources that had previously remained undetected. These appeared to be the only excesses found independently both in the OSA9.0 mosaic and the mosaic obtained with the BAT_IMAGER software (Segreto et al. 2008, 2010). A summary of the properties of the sources is given in Table 2. There we report the best values of the detection significance, source position, and the associated errors. The sources were named according to the standard *INTEGRAL* convention. A mosaic containing all the new sources is shown in Fig. 1.

Table 2. Newly discovered *INTEGRAL* sources around AX J1910.7+0917.

Name	RA (deg)	Dec (deg)	Err. (′)	Det.[a] (σ)	Counts[b]	Exp.[c] (Ms)
IGR J19173+0747	289.349	7.785	2.1	10.0	0.15 ± 0.02	3.0
IGR J19294+1327	292.367	13.459	3.4	6.8	0.12 ± 0.02	2.1
IGR J19149+1036	288.73[d]	10.61[d]	1.0[d]	~20[d]	~0.3[d]	2.6

Notes. [(a)] Detection significance in the IBIS/ISGRI mosaic (17−80 keV); [(b)] the count rates in cts/s estimated from the ISGRI mosaic. In this energy band 1 mCrab = 0.28 cts/s; [(c)] effective exposure time; [(d)] these values are affected by large systematic uncertainties related to the presence of GRS 1915-105.

We report in Table 2 only a first-order approximation for the values of IGR J19149+1036 because it is relatively close ($\lesssim$20 arcmin) to the brighter object GRS 1915-105 and a precise determination of the degree of contamination would require a much more detailed analysis. We note, though, that the inferred source position is coincident with the *Einstein* source 2E 1912.5+1031. For IGR J19173+0747 and IGR J19294+1327, we performed a spectral analysis. For IGR J19173+0747, the ISGRI spectrum was well described by a power-law model with $\Gamma = 3.3^{+0.9}_{-0.7}$ ($\chi^2_{\rm red}$/d.o.f. = 0.3/5) and flux of $F_{20-40\ \rm keV} = 5.6 \times 10^{-12}$ erg/cm^2/s. A similar analysis for IGR J19294+1327 gave $\Gamma = 2.6^{+0.8}_{-0.7}$, $F_{20-40\ \rm keV} = 6.5 \times 10^{-12}$ erg/cm^2/s and $\chi^2_{\rm red}$/d.o.f. = 0.4/4.

3.1. Swift/XRT follow-up of the newly discovered sources

Following the discovery of the three new sources reported in the previous section, we asked for follow-up observations (PI L. Stella) in the soft X-ray domain with *Swift*/XRT (0.3−10 keV; Gehrels et al. 2004). At the time of writing, only the follow-up observations in the direction of IGR J19173+0747 and IGR J19294+1327 were carried out. In order to search for the X-ray counterpart of these two sources, we used the best-determined positions and errors in Table 2. We processed all the *Swift*/XRT data with the XRTPIPELINE and the latest calibration files available (caldb v.20091130). All observations were performed in photon-counting mode (PC). Filtering and screening criteria were applied by using FTOOLS (Heasoft v.6.9). We extracted source and background light curves and spectra by selecting event grades of 0−12 for the PC mode, and created the exposure maps for each observation through the XRTEXPOMAP task. We rebinned each spectrum where possible to have at least 20 photons per bin and used the latest spectral redistribution matrices available in the HEASARC calibration database (v.011). Ancillary response files, accounting for different extraction regions, vignetting and PSF corrections, were generated with the XRTMKARF task. For each of the two sources, we determined an improved source position by using the XRTCENTROID task.

3.1.1. IGR J19173+0747

IGR J19173+0747 was observed by *Swift*/XRT starting on 2010 February 22 at 08:07:00, for a total exposure time of 6 ks. An image of the source is shown in Fig. 8. Inside the *INTEGRAL* error circle there is only one soft X-ray source.

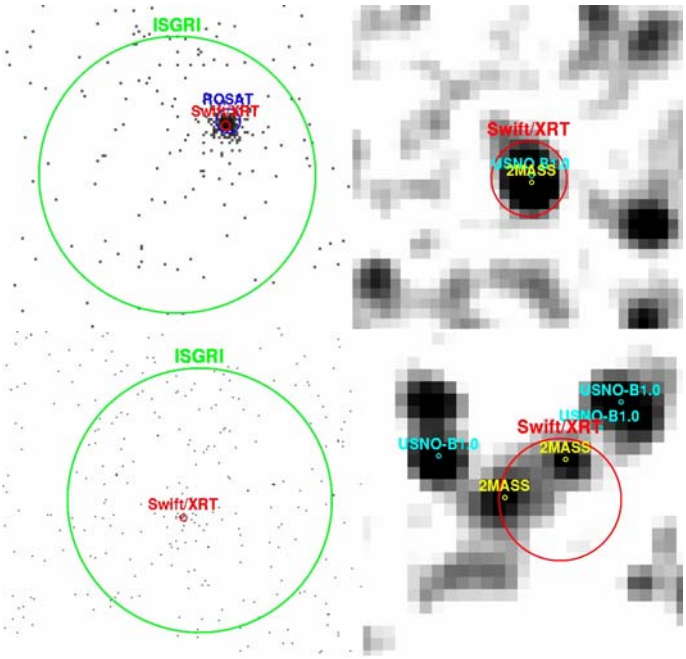

Fig. 8. *Swift*/XRT observations of the newly discovered *INTEGRAL* sources. *Top*: IGR J19173+0747. In this case only one soft X-ray source is found in *Swift*/XRT within the ISGRI error circle. We show on the right the 2MASS infrared image (J band) together with the *Swift*/XRT error circle and the position of the IR and optical counterpart. A positionally coincident *ROSAT* source is also shown. *Bottom*: for IGR J19294+1327 only one very faint soft X-ray excess has been found in the *Swift*/XRT observation (S/N = 3.7). Within the assumed XRT error circle there are two possible IR candidates, but no optical counterpart has been found (see the electronic version of the paper for the colored image).

The spectrum of the source could be well fitted by an absorbed power-law model. We estimated a PL photon index of $\Gamma = 0.6 \pm 0.2$ and obtained an upper limit on the absorption column density of $N_{\rm H} < 6 \times 10^{21}$ cm^{-2} (90% c.l.). The corresponding flux is $(6^{+1.0}_{-1.5}) \times 10^{-12}$ erg/cm^2/s (0.5−10 keV). Extrapolating this flux to the 20−40 keV band would predict a much higher flux ($\sim 2.8 \times 10^{-11}$ erg/cm^2/s) than the one observed with IBIS/ISGRI (5.6×10^{-12} erg/cm^2/s, see Sect. 3). This, together with the different photon index derived in the two energy ranges, suggests a break in the spectrum at energies between 10 and 20 keV, or alternatively a variability of the source. We obtained a refined source position at $\alpha_{\rm J2000}$ = 19$^{\rm h}$17$^{\rm m}$20$^{\rm s}$.8 and $\delta_{\rm J2000}$ = 07°47′51″.1, with an associated uncertainty of 3.8 arcsec (90% c.l.). This position is consistent with that of the *ROSAT* source 1RXS J191720.6+074755 (Voges et al. 1999). The count rate of the source is 0.04 ± 0.01 cts/s in the 0.1−2.4 keV band. By assuming the spectral shape determined above, we checked with the online tool WEBPIMMS that the *ROSAT* countrate would correspond to a flux compatible with that of *Swift*/XRT. Inside the *Swift*/XRT error circle we found only one possible NIR and optical counterpart. The NIR counterpart is 2MASS J19172078+0747506, characterized by J = 13.945 ± 0.031, H = 13.520 ± 0.030, and K = 13.311 ± 0.043. The optical counterpart is USNO-B1.0 0977-0532587 ($R1$ = 15.46, $B1$ = 16.91, $R2$ = 14.99, $B2$ = 16.14, I = 14.78). We queried the FIRST Survey and the NVSS catalogs in search for a radio counterpart, but did not find any obvious candidate.

3.1.2. IGR J19294+1327

IGR J19294+1327 was observed by *Swift*/XRT twice, on 2010 February 22 beginning at 23:59:01 and on 2010 February 26 beginning at 10:16:01. The total exposure time was 7.4 ks. In the *Swift*/XRT FOV only one very faint X-ray source is visible within the ISGRI error circle (S/N = 3.7, see Fig. 8). Given the relatively low S/N ratio, other observations are needed to confirm this detection. Assuming that this is the real counterpart of the *INTEGRAL* source, we estimated its best position at $\alpha_{\rm J2000}$ = 19$^{\rm h}$29$^{\rm m}$29$^{\rm s}$.80 and $\delta_{\rm J2000}$ = 13°27′05″.44 (associated error of 5.0 arcsec). The estimated source count rate was $(4.0 \pm 1.1) \times 10^{-3}$ cts/s, corresponding to an X-ray flux of 3×10^{-13} erg/cm^2/s (0.3−10 keV, we assumed $N_{\rm H} = 7.1 \times 10^{21}$ cm^{-2}, and $\Gamma = 1.5$). This low flux, compared to that measured in the 20−40 keV band, suggests that either the source is intrinsically very faint in the 0.3−10 keV range, or that it is a strongly variable source. Within the *Swift*/XRT error circle we found the two possible NIR counterparts 2MASS J19292976+1327087 (J = 16.075 ± 0.143, H = 15.187 ± 0.150, K = 14.761 ± 0.133) and 2MASS J19293011+1327056 (J = 16.018 ± 0.137, H = 14.725 ± 0.119, K = 13.803 ± 0.101). No cataloged optical or radio counterpart was found at these positions.

4. Discussion and conclusions

We reported on the analysis of all available X-ray observations carried out with *INTEGRAL*, *XMM-Newton*, *Chandra*, and *ASCA* that included AX J1910.7+0917 in the instruments' FOVs. The information we could extract from these data showed that in the soft X-ray energy band (0.5−10 keV) the source is clearly variable. The highest dynamic range in the X-ray flux we could investigate with all available observations and instruments is $\gtrsim$60 (see Table 1). The highest flux was recorded during the *XMM-Newton* observations, which also provided an improved source position and the first detailed characterization of the spectrum of the source. In the *XMM-Newton* data, AX J1910.7+0917 appeared to be variable on a relatively short timescale (hundreds of seconds) and the 0.5−10 keV X-ray spectrum could be well fitted with an absorbed power-law model. In the second available *XMM-Newton* observation, we also found that an iron line was required to fit the spectrum of the source. The centroid of the line is at ∼6.4 keV, consistent with fluorescence origin from cold iron (likely due to iron material in a ionization state not higher that Fe XX). The absorption column density measured in the different X-ray observations showed only minor changes and remained always much higher than that expected in the direction of the source ($\sim 1.5 \times 10^{22}$ cm^{-2}). The power-law photon index was constant (to within the errors) in all data we analyzed. In the hard X-ray energy band (17−80 keV) the source was characterized by a mean X-ray flux of a few 10^{-12} erg/cm^2/s. No evidence was found in the *XMM-Newton* and *INTEGRAL* data for a coherent periodicity that could be associated with the spin period of a neutron star hosted in this system or an orbital period. The improved X-ray position obtained thanks to the *XMM-Newton* observations also allowed us to search for possible counterparts in different energy bands (optical, infrared, radio). In Sect. 2.1.5 we suggested a possible association between AX J1910.7+0917 and the object 2MASS J19104360+0916291, which is the closest classified object to the *XMM-Newton* position. No obvious counterpart in the optical and radio band could be identified.

The available X-ray data on AX J1910.7+0917 do not allow for an unambiguous classification of this source. Its position, relatively close to the Galactic plane, favors the

hypothesis of a Galactic source, and we discuss below a few different possibilities. A relevant feature for investigating the nature of AX J1910.7+0917 is the iron line visible in the *XMM-Newton* observations. The width and the centroid of the line are compatible with a fluorescence origin and thus suggest that AX J1910.7+0917 is likely part of a binary system. Similar iron lines are indeed unlikely to appear in the X-ray spectra of isolated compact objects and magnetars (see, e.g. Mereghetti 2008). The apparent lack of intrinsic broadening would also argue against AX J1910.7+0917 being a low-mass X-ray binary (Bhattacharyya & Strohmayer 2007, and references therein). Among the different subclasses of cataclysmic variables (for a review see Warner 1995, and references therein), polar systems are hardly detected in the ISGRI energy band. Furthermore, for these systems a variability in flux of order ~60 is uncommon. Similar arguments apply to the intermediate polar case. These sources sometimes display emission above 20 keV, but they are known to be generally persistent objects in the soft energy band (0.5−10 keV). We also suggest that the X-ray properties of AX J1910.7+0917 are not compatible with those of novae sources (Warner 1995). A more likely possibility is that AX J1910.7+0917 is a new member of the high-mass X-ray binaries (HMXB) discovered by *INTEGRAL*. According to this interpretation, the iron line observed in the *XMM-Newton* spectrum could originate from irradiation of cold iron in the wind of a massive companion. The analysis conducted in Sect. 2.1.5 on the nature of the possible IR counterpart to AX J1910.7+0917 and the low Galactic latitude of the source would also support this interpretation. However, the association of AX J1910.7+0917 with the class of the HMXBs would still face some difficulties. Among the different subclasses of HMXBs observed by *INTEGRAL*, neither the classical supergiants (see e.g., Walter et al. 2006) nor the SFXT (Sguera et al. 2005) have a behavior fully compatible with that of AX J1910.7+0917. On the one hand, the variability in the X-ray flux reported in Table 1 for the different observations available clearly shows that AX J1910.7+0917 is not a persistent source as expected for the classical supergiant HMXBs. On the other hand, the non detection in the ISGRI data of some bright and short flares typical of the SFXT sources argues against this interpretation. Another possibility is that AX J1910.7+0917 is a Be X-ray binary, and the *XMM-Newton* observation luckily caught the source during an outburst. According to this interpretation we would expect a somewhat higher flux during this period in the *INTEGRAL* observations of AX J1910.7+0917. We checked that no simultaneous *INTEGRAL* and *XMM-Newton* observations were available, and in the closest ISGRI data (obtained about 7 days before and after the *XMM-Newton* observations) AX J1910.7+0917 was detected with a count rate compatible with the average one. We concluded that if the high flux measured in the *XMM-Newton* data corresponded to an outburst, then this should have lasted less than 10 days. This could still be compatible with the durations of the outbursts observed from Be systems. Extrapolating the *XMM-Newton* spectrum in the ISGRI energy band (17−80 keV), we estimated that a similar bright event should correspond to an ISGRI count rate of 1.5−2 cts/s. We searched for similar events in all available ISGRI data by using a 5-day binned lightcurve and found no evidence for such bursts. During the 2200 days spanned by the ISGRI data the source was effectively monitored for approximately 415 days. This suggests that AX J1910.7+0917 should spend <80% of the time in the bright X-ray state observed by *XMM-Newton*. Additional pointed observations in X-rays with *XMM-Newton* and *Chandra*, as well as follow-up observations in different energy bands, are required in order to firmly establish the nature of AX J1910.7+0917.

Besides carrying out a detailed study of AX J1910.7+0917 in X-rays, we also report the discovery of three new hard X-ray sources in the IBIS/ISGRI FOV around AX J1910.7+0917. These sources were independently detected with the OSAv9.0 and the BAT_IMAGER software (Segreto, priv. comm.) and are the only excesses appearing in both the mosaics extracted around AX J1910.7+0917 with the two software packages. As we showed in Sect. 3, a detailed study of 2E 1912.5+1031 could not be carried out because of the likely contamination in the *INTEGRAL* data by the bright source GRS 1915-105 and the lack of proper follow-up with *Swift*. A more refined analysis of this source will be reported elsewhere. For the two new *INTEGRAL* sources IGR J19173+0747 and IGR J19294+1327, we identified a counterpart in the soft X-ray energy band (0.3−10 keV) thanks to dedicated *Swift* observations (see Sect. 3), and searched for possible cataloged optical and infrared counterparts. However, owing to the relative faintness of the sources in the hard X-ray band ($<10^{11}$ erg/cm^2/s in the 17−80 keV band) and the short exposure time of the *Swift*/XRT observations, a clear classification of the two sources is still premature, and other observations are required in order to determine their nature.

Acknowledgements. We thank G. Cusumano for sharing the information on the *Swift*/BAT data on AX J1910.7+0917, A. Segreto for the information on the results obtained with BAT_IMAGER software, and M. Falanga for useful discussions. We thank the referee P. R. den Hartog for his useful comments that improved the content of this paper. L.S. acknowledges financial support from ASI.

References

Bhattacharyya, S., & Strohmayer, T. E. 2007, ApJ, 664, L103
Bird, A. J., Bazzano, A., Bassani, L., et al. 2010, VizieR Online Data Catalog, 218, 60001
Courvoisier, T., Walter, R., Beckmann, V., et al. 2003, A&A, 411, L53
Garmire, G. P., Bautz, M. W., Ford, P. G., Nousek, J. A., & Ricker, Jr., G. R. 2003, in Society of Photo-Optical Instrumentation Engineers (SPIE) Conf. Ser., ed. J. E. Truemper, & H. D. Tananbaum, 4851, 28
Gehrels, N., Chincarini, G., Giommi, P., et al. 2004, ApJ, 611, 1005
Hertz, P., & Grindlay, J. E. 1988, AJ, 96, 233
Jansen, F., Lumb, D., Altieri, B., et al. 2001, A&A, 365, L1
Lebrun, F., Leray, J. P., Lavocat, P., et al. 2003, A&A, 411, L141
Lund, N., Budtz-Jørgensen, C., Westergaard, N. J., et al. 2003, A&A, 411, L231
Makishima, K., Tashiro, M., Ebisawa, K., et al. 1996, PASJ, 48, 171
Mereghetti, S. 2008, A&ARv, 15, 225
Miceli, M., Decourchelle, A., Ballet, J., et al. 2006, A&A, 453, 567
Negueruela, I., & Schurch, M. P. E. 2007, A&A, 461, 631
Ohashi, T., Ebisawa, K., Fukazawa, Y., et al. 1996, PASJ, 48, 157
Segreto, A., Cusumano, G., La Parola, V., et al. 2008, in Proceedings of the 7th INTEGRAL Workshop
Segreto, A., Cusumano, G., Ferrigno, C., et al. 2010, A&A, 510, A47
Sguera, V., Barlow, E. J., Bird, A. J., et al. 2005, A&A, 444, 221
Skrutskie, M. F., Cutri, R. M., Stiening, R., et al. 2006, AJ, 131, 1163
Sugizaki, M., Mitsuda, K., Kaneda, H., et al. 2001, ApJS, 134, 77
Tanaka, Y., Inoue, H., & Holt, S. S. 1994, PASJ, 46, L37
Ubertini, P., Lebrun, F., Di Cocco, G., et al. 2003, A&A, 411, L131
Voges, W., Aschenbach, B., Boller, T., et al. 1999, A&A, 349, 389
Walter, R., Zurita Heras, J., Bassani, L., et al. 2006, A&A, 453, 133
Warner, B. 1995, Cambridge Astrophysics Series, 28
Watson, M. G., Schröder, A. C., Fyfe, D., et al. 2009, A&A, 493, 339
Winkler, C., Courvoisier, T., Di Cocco, G., et al. 2003, A&A, 411, L1